TsAGI Science Journal, 48(1): 31–42 (2017)

APPLICATION OF VARIOUS MODELS OF TURBULENCE FOR CALCULATION OF INCOMPRESSIBLE INTERNAL FLOWS

P.A. Baranov,[1] S.V. Guvernyuk,[2] M.A. Zubin,[2] S.A. Isaev,[3] & A.E. Usachov[4,*]

[1]*Battery Company "RIGEL," 38 Professor Popov Str., Saint Petersburg, 197376, Russian Federation*

[2]*Institute of Mechanics, Lomonosov Moscow State University, 1 Michurinskii prospekt, Moscow, 119192, Russian Federation*

[3]*Saint Petersburg State University of Civil Aviation, 38 Pilotov Str., Saint Petersburg, 196210, Russian Federation*

[4]*Central Aerohydrodynamic Institute (TsAGI), 1 Zhukovsky Str., Zhukovsky, Moscow Region, 140180, Russian Federation*

*Address all correspondence to: A.E. Usachov, Central Aerohydrodynamic Institute (TsAGI), 1 Zhukovsky Str., Zhukovsky, Moscow Region, 140180, Russian Federation, E-mail: uzts@tsagi.ru

Five models of turbulence are used for numerical simulation of the incompressible internal turbulent flow in a plane channel with a cylindrical cavity on the wall. The results of the numerical simulation are compared with the experimental data at Reynolds number $Re = 1.34 \times 10^5$. Conclusions about the applicability of turbulence models for similar types of flow are made based on comparison of the calculation and experimental data.

KEY WORDS: *numerical simulation, differential turbulence models, comparison with the experiment*

1. INTRODUCTION

A large variety of differential turbulence models are available nowadays, which are used to describe different types of turbulent flow. The purpose of this investigation is to compare five current turbulence models that are widely applied in practice for numerical simulation of internal two-dimensional turbulent flows. A plane channel with an open cylindrical cavity on the wall was chosen as the flow type to study. The problem was formulated as a comparison of the numerical simulation data obtained by various turbulence models and with the experimental data.

2. GENERAL EQUATIONS AND SOLUTION METHOD

The total system of equations describing the motion of viscous fluid in the Cartesian coordinate system can be presented in tensor form as follows [1]:

1948–2590/17/$35.00

- Continuity equation

$$\frac{\partial U_j}{\partial x_j} = 0 \tag{1}$$

- Equation of momentum variation (Reynolds-averaged Navier–Stokes equation)

$$\rho \frac{\partial U_i}{\partial t} + \rho U_j \frac{\partial U_i}{\partial x_j} = -\frac{\partial p}{\partial x_i} + \mu \frac{\partial^2 U_i}{\partial x_j \partial x_i} - \frac{\partial p \overline{u_i' u_j'}}{\partial x_j} \tag{2}$$

where t is time; x_i is the Cartesian coordinate (i = 1, 2, 3); U_i is the fluid flow averaged velocity component in the x_i direction; p is the averaged static pressure; ρ is the density; and μ is the dynamic viscosity coefficient.

In accordance with the Boussinesq hypothesis, the Reynolds stresses on the right-hand side of the equation are simulated as follows:

$$-\rho \overline{u_i' u_j'} = \mu_t \left(\frac{\partial U_i}{\partial x_j} + \frac{\partial U_j}{\partial x_i} \right) - \frac{2}{3} \left(\mu_t \frac{\partial U_i}{\partial x_i} + \rho k \right) \delta_{ij} \tag{3}$$

where $k = \overline{u_i' u_i'}/2$ is the kinetic energy of turbulence fluctuations; and μ_t is the dynamic coefficient of turbulent viscosity determined in accordance with the chosen turbulence model.

To close the Reynolds-averaged Navier–Stokes equations, the Spalart–Allmares (SA) turbulence model with correction of the source term [2], realizable k-ε turbulence model [3], shear stress transport (SST) k-ω Menter model [4,5], transition SST k-ω model [6], and turbulence model for Reynolds stress model (RSM) were applied [7–12]. The operability of the turbulence models was estimated by comparing the calculation and experimental data by solving the problem of viscous fluid motion in a plane-parallel channel with a vortex cell in the form of a circular cut in its wall [13].

3. EXPERIMENTAL FACILITY AND TEST PROCEDURE

The experimental investigation of the flow in a channel with a crosswise cylindrical cavity was performed at the Institute of Mechanics, Lomonosov Moscow State University, in a special vortex cell facility, ViYa [Fig. 1(a)]. The facility is a small-sized direct wind tunnel, in which the air flow is generated by pressure fan 1. In order to flatten and stabilize the flow, elongated settling chamber 2 is situated in front of nozzle 3, with a honeycomb and a fine-meshed screen for disturbance damping installed in this settling chamber.

The settling chamber smoothly meets plane-contoured subsonic nozzle 3 with compression ratio 4, which is joined to the facility operating channel 4 made of acrylic glass with a 0.05-m-high and 0.08-m-wide rectangular cross section. Replaceable units with cylindrical cavities of different diameters d at the same inlet length of $L = 0.052$ m are installed on the lower horizontal wall of the channel [Figs. 1(b) and 1(c)]. The upper wall of the channel can be deflected by angle α up to 10°, which enables the longitudinal pressure gradient to be regulated in the vicinity of the cell. The propeller and the nozzle ensure uniform flow in channel inlet section $x = x_*$ with velocity U in the range from 1.5 to 50 m/s. The Reynolds number defined by L and U varies within $6 \times 10^3 < \mathrm{Re} < 1.8 \times 10^5$.

A uniform cross-section channel ($\alpha = 0$) with an insert of diameter $d = 0.06$ m at flow velocity $U = 36$ m/s ($\mathrm{Re} = 1.34 \times 10^5$) was used in the present investigation. The values of L

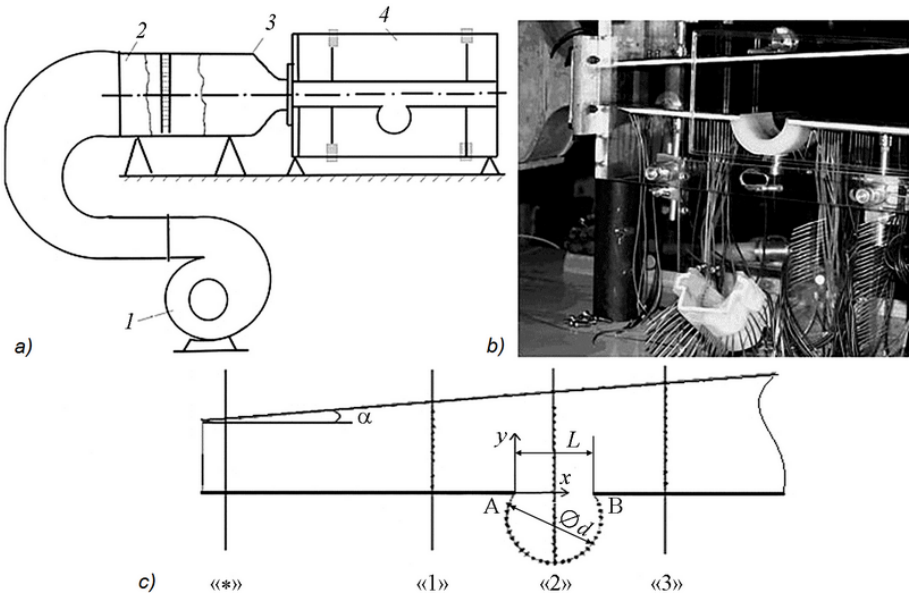

FIG. 1: Experimental facility (ViYa-1)

and U were chosen as typical scales of the length and velocity. Figure 1(c) shows the typical cross sections, where the measurements were performed. The dimensionless coordinates of typical cross sections are given in Table 1. The level of turbulence fluctuations $\varepsilon(y) = \sqrt{\overline{u'^2}}$ in channel inlet section $x = x_*$ was measured by hot-wire anemometer DISA A-55. Outside of the boundary layer, the value of ε was on the level of 1.6%.

The distribution of dynamic pressure $q = \rho u^2/2$ was determined by the difference between the total and static pressures. In order to measure the pressures, the differential probes [obtained from Honeywell (Morris Plains, New Jersey)] of various ranges were used (±62.5, ±122.5, and 250 mm H_2O column); their measurement error was 0.5%–1%. Measurement of the total and static pressures in the flow and near the surfaces in various cross sections of the channel was performed by microprobes, which were displaced by a coordinate spacer with a micrometer screw allowing controlled displacement with accuracy up to 0.05 mm. In addition, the static pressure was measured using pressure holes on the channel walls.

The static pressure measurements in three cross sections of the channel [see Fig. 1(c)] enabled the following conclusions to be made:

1. The weak effect of the side (front and rear) walls of the channel can be neglected, which is confirmed by the almost constant pressure across the width of the channel measured by the pressure holes on the channel lower wall and cylindrical cavity bottom.

TABLE 1: Dimensionless coordinates of typical cross sections

$\|AB\|$	x_*	x_1	x_2	x_3
1	–3.73	–1.04	0.5	1.94

2. There is almost constant static pressure throughout the channel height in the cross sections in front of and behind the cavity.

3. There is the presence of a strong vortex flow in the cylindrical cavity, which is indicated by a typical drop in static pressure on the side walls of the channel in the vicinity of the cavity center.

The first peculiarity of the flow from the aforementioned conclusions was determined in the process of choosing the two-dimensional computational model.

The presence of a favorable static pressure gradient in the channel in front of and behind the cavity is the consequence of the displacing effect of the boundary layers. The incoming boundary layer velocity profile recovered by the measured dynamic pressure in section $x = x_1$ along vertical coordinate y is shown in Fig. 2(a). The following integral parameters were calculated using the Bézier spline approximations of this profile:

$$\delta^* = \int_0^\delta \left(1 - \frac{u_1(y)}{u_{1e}}\right) dy, \quad \delta^{**} = \int_0^\delta \left(1 - \frac{u_1(y)}{u_{1e}}\right) \frac{u_1(y)}{u_{1e}} dy$$

where $\delta^* = 0.015$ is the displacement thickness and $\delta^{**} = 0.0099$ is the momentum thickness (in which u_{1e} is the constant velocity flow outside of the boundary layer in section $x = x_1$). Figure 2(b) shows the profile $u_2(y)/u_{2e}$ in the section passing through the cavity center, which is constructed in a similar way using the dynamic pressure measurement data. The typical structural elements of the separation flow in the cavity are well seen, namely, the displacement layer, vortex core, and cyclic boundary layer.

4. SPALART–ALLMARES MODEL FOR EDDY VISCOSITY

The SA model [2] is a one-parameter model with one differential equation for turbulent viscosity, which does not require calculation of the relative length scale. The model was constructed particularly for aerospace systems calculations and predicting the parameters of wall flows, and has been proven to be good when calculating boundary layers with adverse pressure gradients.

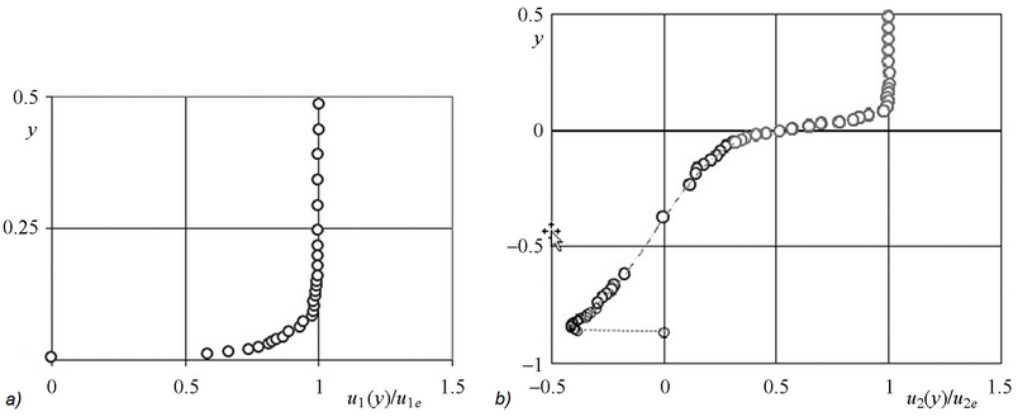

FIG. 2: Velocity profiles in the control sections: (a) $x = x_1$; (b) $x = x_2$

For internal aerodynamics problems the SA model has been applied successfully in modeling the flow in turbomachines. The SA model is a low Reynolds number model that requires appropriate resolution of the boundary-layer near-wall zone. In the FLUENT software tool [15] it is used in combination with the near-wall functions in cases in which relatively coarse meshes are applied. Note that the model is less sensitive to numerical errors when unstructured meshes are used near the walls; however, it is not quite impeccable, and in particular cannot predict the decay of homogeneous isotropic turbulence.

The differential equation for calculating turbulent viscosity coefficient $\tilde{\nu}$, written in Cartesian coordinates x_i, in combination with the algebraic expressions for auxiliary functions and model constants is formulated as follows:

$$\frac{\partial(\rho\tilde{\nu})}{\partial t}+\frac{\partial(\rho\tilde{\nu}U_i)}{\partial x_i}=G_{\tilde{\nu}}+\frac{1}{\sigma_{\tilde{\nu}}}\left\{\frac{\partial}{\partial x_j}\left[(\mu+\rho\tilde{\nu})\frac{\partial\tilde{\nu}}{\partial x_j}\right]+C_{b2}\rho\left(\frac{\partial\tilde{\nu}}{\partial x_j}\right)^2\right\}-Y_{\tilde{\nu}}$$

$$\mu_t=\rho\tilde{v}f_{\nu 1} \tag{4}$$

where $G_{\tilde{\nu}}$ is the turbulent viscosity generation; $Y_{\tilde{\nu}}$ is the turbulent viscosity dissipation; and constants $C_{b2}=0.622$ and $\sigma_{\tilde{\nu}}=2/3$. The article format does not allow demonstrating all of the equations for the turbulence models in full; therefore, here we only present the general equations that provide the model overview. The exact equations of the turbulence models are given in Refs. [2–12].

5. REALIZABLE k-ε MODEL

The realizable k-ε model [3] term means that, in contrast to the high Reynolds number analog, this model contains restrictions on normal stresses that are in accordance with the physics of turbulent flows. It is important to avoid negative values of eddy viscosity for flows with high gradients. This is achieved by introducing a functional dependence instead of constant C_μ, and thus the formula for determining the turbulent viscosity is corrected.

The new transport equation for turbulent energy dissipation rate ε is derived from the exact transport equation of root-mean-square vorticity fluctuations:

$$\frac{\partial(\rho k)}{\partial t}+\frac{\partial(\rho U_i k)}{\partial x_i}=\frac{\partial}{\partial x_j}\left[\left(\mu+\frac{\mu_t}{\sigma_k}\right)\frac{\partial k}{\partial x_j}\right]+G_k-\rho\varepsilon$$

$$\frac{\partial(\rho\varepsilon)}{\partial t}+\frac{\partial(\rho U_i\varepsilon)}{\partial x_i}=\frac{\partial}{\partial x_j}\left[\left(\mu+\frac{\mu_t}{\sigma_\varepsilon}\right)\frac{\partial\varepsilon}{\partial x_j}\right]+\rho C_1G_k-\rho C_2\frac{\varepsilon^2}{k+\sqrt{\nu\varepsilon}}+C_{1\varepsilon}\frac{\varepsilon}{k}C_{3\varepsilon}G_b \tag{5}$$

where G_k is the turbulence kinetic energy generation; and constants $\sigma_k=1$, $\sigma_\varepsilon=1.2$, and $C_2=1.9$.

6. MENTER'S SHEAR STRESS TRANSPORT TURBULENCE MODEL

Menter's SST model does not only couple the widespread k-ω and k-ε models, but also takes into account the shear stress transport [4,5]. The conventional k-ω model and the transformed k-ε model are coupled by the mixing function, which is constructed in such a way that it takes unit value in the near-wall region, that is, the standard k-ω model is activated in it, and it equals zero far from the wall, and then the transformed k-ε model predominates. The SST model is supplemented by a damped term with cross-coupling derivatives in the equation for ω. The

turbulent viscosity is determined by taking into account the turbulent shear stress transport within the Johnson–King approach. There is a certain variation of the model constants from their values in the original models. Relatively recently, Menter introduced corrections into the SST k-ω model, which had been made based on 10 years of experience of employing it [5]. Instead of the vorticity Ω modulus, the invariant strain-rate tensor modulus $S = |S_{ij}| = \sqrt{2S_{ij}S_{ij}}$ is used in the expression for eddy viscosity. Finally, Menter's SST model is implemented in the following form:

$$\frac{\partial(\rho k)}{\partial t} + \frac{\partial(\rho U_i k)}{\partial x_i} = \frac{\partial}{\partial x_j}\left[\Gamma_k \frac{\partial k}{\partial x_j}\right] + G_k - Y_k$$

$$\frac{\partial(\rho\omega)}{\partial t} + \frac{\partial(\rho U_i \omega)}{\partial x_i} = \frac{\partial}{\partial x_j}\left[\Gamma_\omega \frac{\partial \omega}{\partial x_j}\right] + G_\omega - Y_\omega + D_\omega \tag{6}$$

where G_ω is the generation of dissipation of kinetic turbulence ω per unit k; Y_k is the dissipation of turbulence kinetic energy; Y_ω is the dissipation of kinetic turbulence ω; $\Gamma_k = \mu + (\mu_t/\sigma_k)$; $\Gamma_\omega = \mu + (\mu_t/\sigma_\omega)$; and D_ω is the cross-diffusion term.

7. TRANSITION SST MODEL

One of the latest modifications of Menter's SST model is the four-equation turbulence model that takes into account the laminar–turbulent transition [6]. Previous low Reynolds number turbulence models did not take into account many important factors affecting the laminar–turbulent transition in the boundary layer, namely, the external flow turbulence level, presence of pressure gradients, and wall roughness. An attempt to take into account some of these factors is made in the proposed turbulence model. For this purpose, two supplementary differential equations for flow intermittency γ and the local Reynolds number calculated by momentum thickness Re_θ are introduced. The transport equation for flow intermittency γ is written as follows:

$$\frac{\partial(\rho\gamma)}{\partial t} + \frac{\partial(\rho U_j \gamma)}{\partial x_j} = P_{\gamma 1} - E_{\gamma 1} + P_{\gamma 2} - E_{\gamma 2} + \frac{\partial}{\partial x_j}\left[\left(\mu + \frac{\mu_t}{\sigma_\gamma}\right)\frac{\partial \gamma}{\partial x_j}\right]$$

The equation for transition Reynolds number $\mathrm{Re}_{\theta t}$:

$$\frac{\partial\left(\rho\widetilde{\mathrm{Re}_{\theta t}}\right)}{\partial t} + \frac{\partial\left(\rho U_j \widetilde{\mathrm{Re}_{\theta t}}\right)}{\partial x_j} = P_{\theta t} + \frac{\partial}{\partial x_j}\left[\sigma_{\theta t}\left(\mu + \frac{\mu_t}{\sigma_\gamma}\right)\frac{\partial \widetilde{\mathrm{Re}_{\theta t}}}{\partial x_j}\right] \tag{7}$$

where $P_{\gamma 1}$, $E_{\gamma 1}$, $P_{\gamma 2}$, $E_{\gamma 2}$, and $P_{\theta t}$ are the source terms; and constants $\sigma_\gamma = 1.0$ and $\sigma_{\theta t} = 2.0$.

8. EQUATIONS FOR REYNOLDS STRESSES

To close the Reynolds-averaged Navier–Stokes equations it is possible to use the transport equations for Reynolds stresses. They are given here in the most general form [7–12]:

$$\begin{aligned}\frac{\partial}{\partial t}\left(\rho\overline{u_i' u_j'}\right) + \frac{\partial}{\partial x_k}\left(\rho u_k \overline{u_i' u_j'}\right) &= -\frac{\partial}{\partial x_k}\left[\rho\overline{u_i' u_j' u_k'} + \overline{p\left(\delta_{kj}u_i' + \delta_{ik}u_j'\right)}\right] \\ + \frac{\partial}{\partial x_k}\left[\mu\frac{\partial\overline{\left(u_i' u_j'\right)}}{\partial x_k}\right] - \rho\left(\overline{u_i' u_k'}\frac{\partial u_j'}{\partial x_k} + \overline{u_i' u_k'}\frac{\partial u_j}{\partial x_k}\right) &+ \overline{p\left(\frac{\partial u_i'}{\partial x_j} + \frac{\partial u_j'}{\partial x_i}\right)} - 2\mu\overline{\frac{\partial u_i'}{\partial x_k}\frac{\partial u_j'}{\partial u_k}}\end{aligned} \tag{8}$$

where δ_{kj} is the delta function. Some terms on the right-hand side of the transport equation for Reynolds stresses are not determined. They are defined using additional relationships. This refers to the turbulent diffusion transport and pressure correlations. To close them, additional relationships with application of the equations for the turbulence kinetic energy and its dissipation are used [9–12].

9. NUMERICAL SOLVER

Numerical simulation was performed using the VP2/3 software package (Saint Petersburg and Moscow). The differential equations were solved by the well-proven numerical control volume method [14], which allows constructing conservative discrete schemes for non-orthogonal curvilinear meshes with cells of various shapes. Both the steady-state and unsteady Reynolds-averaged Navier–Stokes equations were solved by the control volume method [14].

For discretization of convective fluxes through the control volume faces, the second-order upwind schemes were used [15]. The pressure was calculated using the semi-implicit methods SIMPLEC (semi-implicit method for pressure linked equations-consistent) based on the SIMPLE procedure suggested by Patankar [16]. Based on this multi-block computational procedure (MCP) technique, the software complex VP2/3 was elaborated, which has been applied successfully in the numerical simulation of different heat-and-mass transfer problems in viscous fluid flows [16].

An unstructured triangular mesh with 137,678 cells was used in the numerical simulation. The minimal distance to the wall was $y = 0.0002$ of the reference length. The control of y^+ value showed that it did not exceed 2 near the wall.

10. RESULTS OF THE NUMERICAL SIMULATION

The results of the numerical simulation of incompressible steady-state flow in the channel with the cylindrical cavity for the Reynolds-averaged Navier–Stokes equations closed by turbulence models (4)–(8) are shown in Figs. 3–7. The fields of velocity vector and paths of the tag particles found in the numerical simulation using various turbulence models are shown in Fig. 3.

The flow modeling in the cylindrical cavity using all three turbulence models provided close results. A recirculation flow with a large eddy in the cavity center arose in the cavity, with a small displacement of the eddy center toward the channel rear wall being observed for the SA turbulence model [Fig. 3(a)]. In addition, when Menter's SST turbulence model [Fig. 3(c)] and the transition SST model [Fig. 3(d)] were used, a small secondary recirculation flow near the leading sharp edge was observed.

The fields of velocity modulus with the same color gradation over the velocity modulus value are shown in Fig. 4. An insignificant discrepancy in the velocity modulus was only observed in the application of the SA turbulence model [Fig. 4(a)]. Figure 5 shows the fields of turbulent viscosity, where turbulent viscosity in the eddy center is observed in all of the considered turbulence models except for the realizable k-ε model. This effect does not coincide with the physical processes in the center of a large eddy; however, it disappears when introducing the correction for the curvature of streamlines in the indicated turbulence models [17].

11. COMPARISON OF THE NUMERICAL AND EXPERIMENTAL RESULTS

Let the results of the calculations of the averaged horizontal velocity component profile in the cylindrical cavity center section performed using various turbulence models be compared with

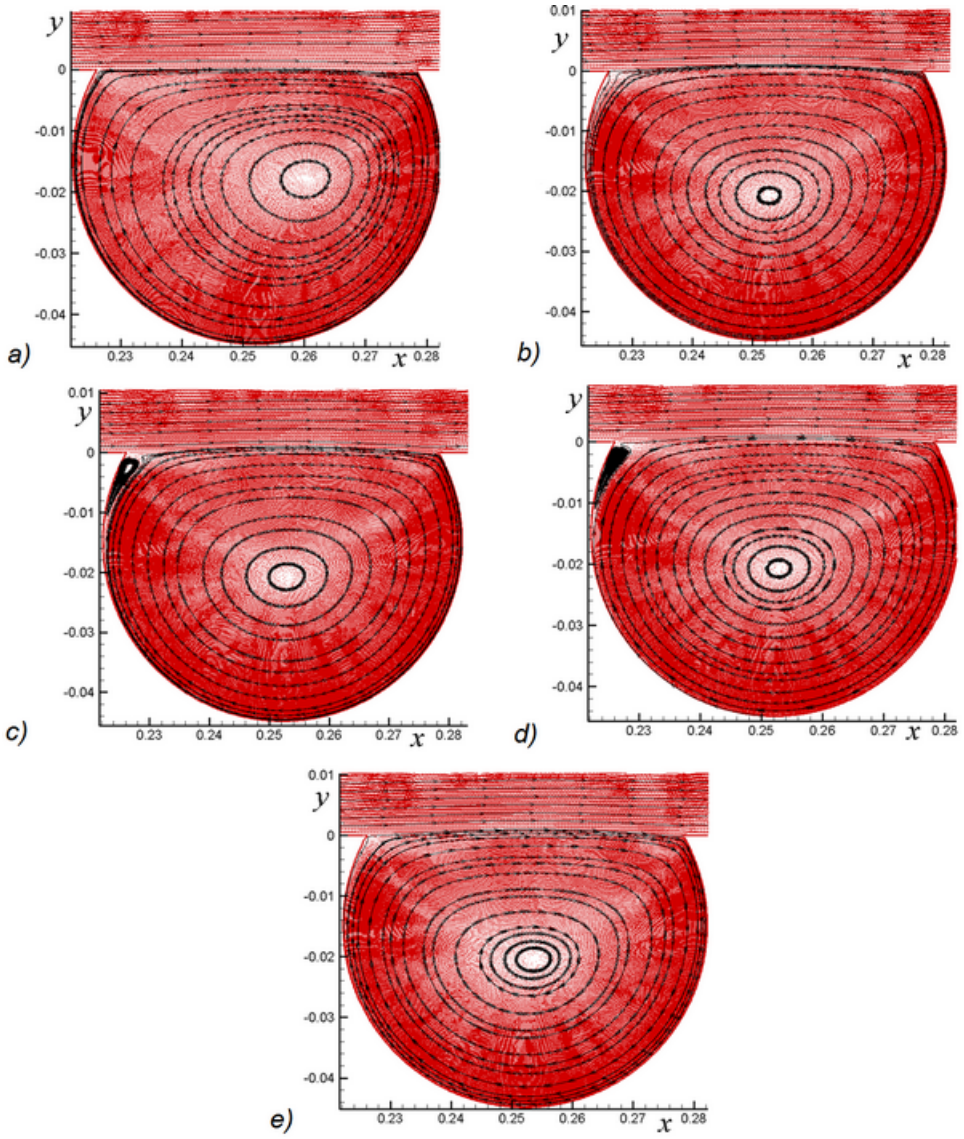

FIG. 3: Velocity vectors and paths of the tag particles: (a) SA turbulence model with correction of the source term; (b) realizable k-ε model of turbulence; (c) Menter's SST k-ω model; (d) transition SST k-ω model; (e) Reynolds stress model

the experimental data. It is necessary to note that all of the results of the computations for averaged horizontal velocity component U obtained by the considered turbulence models are in good agreement with the experimental data (see Fig. 6). Therefore, for more precise analysis, the static pressure distributions on the bottom wall of the channel and cavity obtained in the computations by various turbulence models and experimentally are compared (see Fig. 7). From the analysis of the Figs. 6 and 7, the most satisfactory coincidence is observed in the case of the SST k-ω transition model of Menter with four equations.

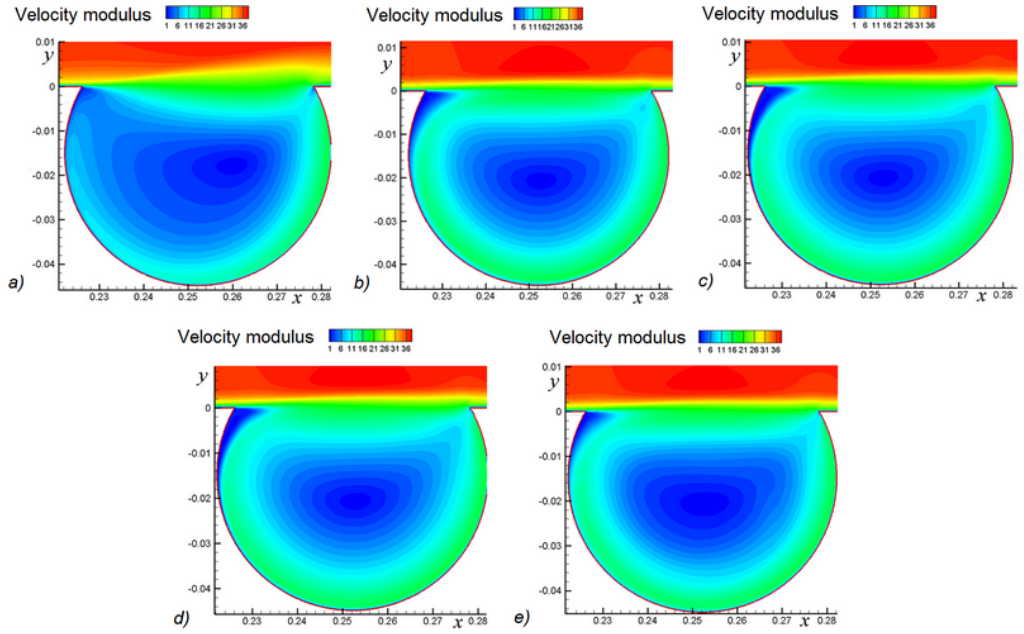

FIG. 4: Field of absolute velocity absolute values: (a) SA turbulence model with correction of the source term; (b) realizable k-ε model of turbulence; (c) Menter's SST k-ω model; (d) transition SST k-ω model; (e) Reynolds stress model

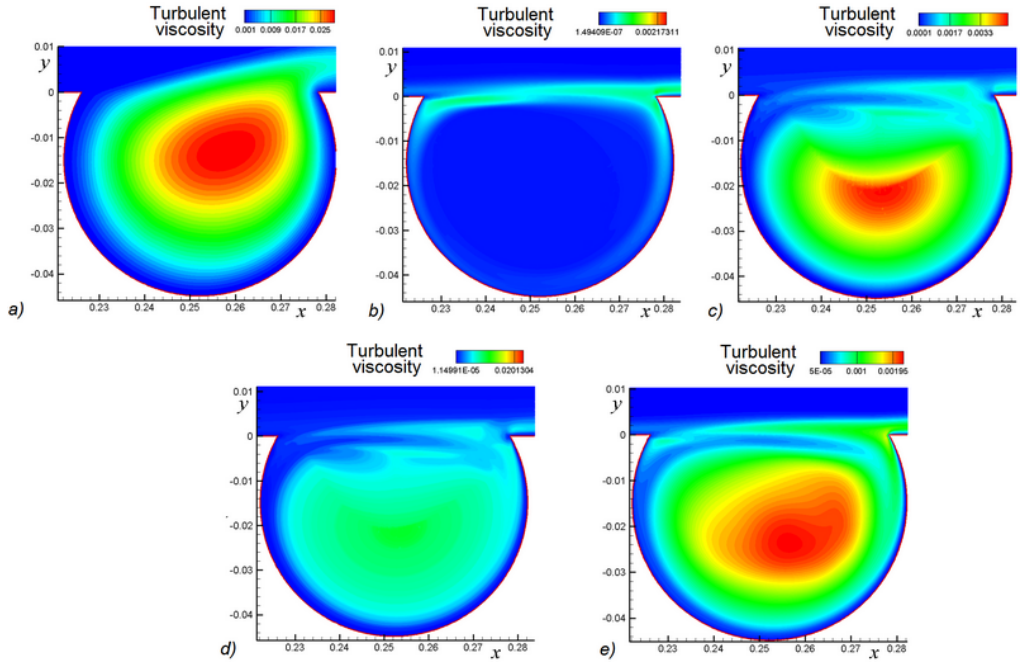

FIG. 5: Turbulent viscosity field: (a) SA turbulence model with correction of the source term; (b) realizable k-ε model of turbulence; (c) Menter's SST k-ω model; (d) transition SST k-ω model; (e) Reynolds stress model

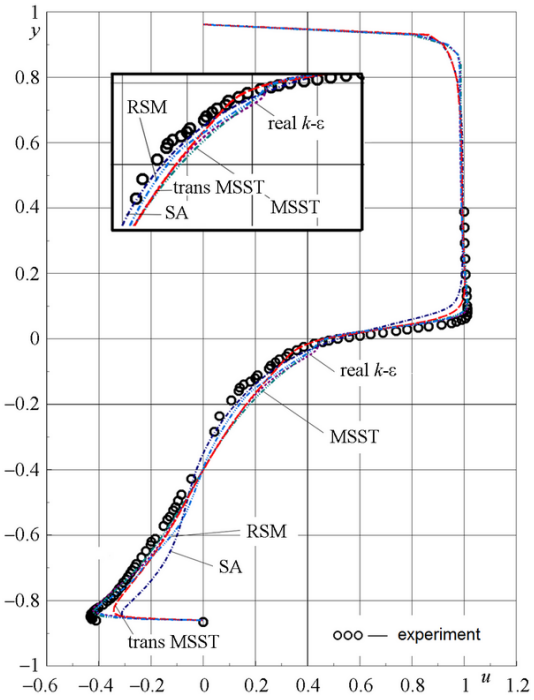

FIG. 6: Comparison of the calculation results of the averaged horizontal velocity component and the experimental results obtained by various turbulence models

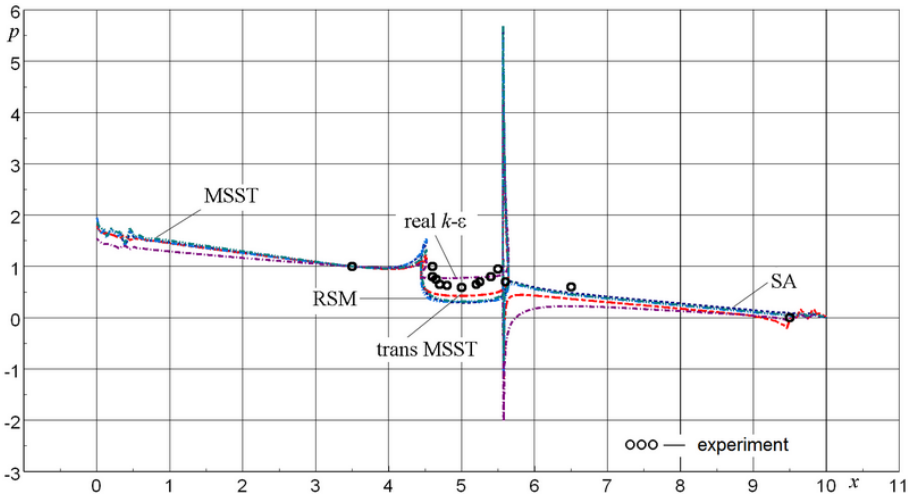

FIG. 7: Comparison of the static pressure distribution over the channel wall and the cavity calculated by various turbulence models and the experimental results

12. CONCLUSIONS

The results of the numerical simulation of five advanced turbulence models (the SA turbulence models with correction of the source term, realizable k-ε turbulence model, SST k-ω

Menter model, transition SST k-ω model, and turbulence RSM model) for incompressible internal steady-state flow in a channel with a cylindrical cavity on its bottom wall were compared. Based on the comparison of the results of the numerical simulation with the experiment for the averaged horizontal velocity component profile and the pressure distribution over the channel bottom wall and cavity bottom in the longitudinal direction, it was shown that the best result was provided by the transition SST turbulence model with four equations.

ACKNOWLEDGMENTS

This study was performed in the framework of TsAGI-Russian Academy of Sciences (RAS) Program 2014-1015 (numerical investigations) and was partially supported by the Russian Science Foundation (RSF), Project No. 14-19-00003 (wind tunnel experiments).

REFERENCES

1. Loitsyanskii, L.G., *Mechanics of Liquids and Gases*, International Series of Monographs in Aeronautics and Astronautics: Division II: Aerodynamics, vol. 6, Amsterdam: Elsevier, 2014.
2. Spalart, P.R. and Allmares, S.R., A one-equation turbulence model for aerodynamic flows, *AIAA Paper 92-0439*, 1992.
3. Shih, T.-H., Liou, W.W., Shabbir, A., Yang, Z., and Zhu, J., A new k-ε eddy–viscosity model for high Reynolds number turbulent flows—model development and validation, *Comput. Fluids*, 24(3):227–238, 1995.
4. Menter, F.R., Zonal two equation k-ω turbulence models for aerodynamic flows, *AIAA Paper 93-2906*, 1993.
5. Menter, F.R., Kuntz, M., and Langtry, R., Ten years of industrial experience with the SST turbulence model, in *Turbulence, Heat and Mass Transfer 4*, K. Hajalic, Y. Nogano, and M. Tummers, Eds., pp. 625–632, New York: Begell House, Inc., 2003.
6. Menter, F.R., Langtry, R.B., Likki, S.R., Suzen, Y.B., Huang, P.G., and Volker, S., A correlation-based transition model using local variables: Part 1—Model formulation, *ASME Paper No. GT2004-53452*, pp. 413–422, 2004.
7. Daly, B.J. and Harlow, F.H., Transport equations in turbulence, *Phys. Fluids*, 13(11):2634–2649, 1970.
8. Gibson, M.M. and Launder, B.E., Ground effects on pressure fluctuations in the atmospheric boundary layer, *J. Fluid Mech.*, 86(3):491–511, 1978.
9. Launder, B.E., Second-moment closure: Present... and future? *Int. J. Heat Fluid Flow*, 10(4):282–300, 1989.
10. Launder, B.E., Reece, G.J., and Rodi, W., Progress in the development of a Reynolds—stress turbulence closure, *J. Fluid Mech.*, 68(3):537–566, 1975.
11. Lien, F.S. and Leschziner, M.A., Assessment of turbulent transport models including non-linear RNG eddy-viscosity formulation and second-moment closure, *Comput. Fluids*, 23(8):983–1004, 1994.
12. Fu, S., Launder, B.E., and Leschziner, M.A., Modeling strongly swirling recirculating jet flow with Reynolds-stress transport closures, in *Proc. of 6th Symposium on Turbulent Shear Flows*, Toulouse, France, 1987.
13. Baranov, P.A., Guvernyuk, S.V., Zubin, M.A., and Isaev, S.A., Numerical and physical modeling of the circulation flow in a vortex cell in the wall of a rectilinear channel, *Fluid Dyn.*, 35(5):663–673, 2000.
14. Baranov, P.A., Guvernyuk, S.V., Isaev, S.A., Soudakov, A.G., and Usachov, A.E., Simulation of periodic vortical structures in the airfoil wake, *TsAGI Sci. J.*, 45(3-4):273–292, 2014.
15. Fluent Inc., *Fluent 6.1 User's Guide*, Lebanon, NH: Fluent Inc., 2003.

16. Isaev, S.A., Baranov, P.A., and Usachov, A.E., *Multiblock Computational Technologies in the VP2/3 Package on Aerothermodynamics*, Saarbrücken, Germany: LAP LAMBERT Academic Publishing, 2013.
17. Isaev, S.A., Baranov, P.A., Kudryavtsev, N.A., Lysenko, D.A., and Usachov, A.E., Complex analysis of turbulence models, algorithms, and grid structures at the computation of recirculating flow in a cavity by means of VP2/3 and fluent packages. Part 2. Estimation of models adequacy, *Thermophys. Aeromech*., 13(1):55–65, 2006.

Pavel Andreevich Baranov, Researcher, Battery Company RIGEL

Sergey Vladimirovich Guvernyuk, Candidate in Physical and Mathematical Sciences, Deputy Director, Institute of Mechanics of the Lomonosov Moscow State University

Mikhail Adolfovich Zubin, Candidate in Physical ad Mathematical Sciences, Leading Researcher, Institute of Mechanics, Lomonosov Moscow State University

Sergey Aleksandrovich Isaev, Doctor in Physical and Mathematical Sciences, Professor, Saint Petersburg State University of Civil Aviation

Aleksandr Evguenyevich Usachov, Doctor in Physical and Mathematical Sciences, Leading Researcher, TsAGI